Precision measurements of B-meson decays at ATLAS

Marek Biros[1]* on behalf of the ATLAS Collaboration

[1]Institute of Particle and Nuclear Physics, Faculty of Mathematics and Physics, Charles University, V Holešovičkách 2, 18000 Prague 8, Czech Republic

Abstract. The precise measurement of the CP-violating phase ϕ_s, the average decay width Γ_s and the difference between the widths of the light and heavy mass eigenstates $\Delta\Gamma_s$ is presented in the $B_s^0 \to J/\psi\phi$ decay channel. Data of pp collisions at $\sqrt{s} = 13$ TeV are used, corresponding to 80.5 fb^{-1} of integrated luminosity collected by the ATLAS detector at the Large Hadron Collider in years 2015–2017. Results are statistically combined with the previous measurement with 19.2 fb^{-1} data with 7 and 8 TeV energy. The measured values are:

$$\begin{aligned}\phi_s &= -0.087 \pm 0.036\ (\text{stat.}) \pm 0.021\ (\text{syst.})\\ \Gamma_s &= 0.6703 \pm 0.0014\ (\text{stat.}) \pm 0.0018\ (\text{syst.})\\ \Delta\Gamma_s &= 0.0657 \pm 0.0043\ (\text{stat.}) \pm 0.0037\ (\text{syst.}).\end{aligned}$$

Moreover, a study estimating the ATLAS detector performance in measuring the CP-violating phase ϕ_s after the HL-LHC upgrade is presented.

1 Introduction

The CP violation (CPV) is a well-known phenomenon in particle physics that can be described within the Standard Model (SM). Ongoing research in this area is focused on the precise measurements of CPV parameters to either detect or reject potential deviations from the SM predictions, that could indicate the presence of potential new phenomena, often referred to as New Physics (NP).

The CPV occurs in the $B_s^0 \to J/\psi\phi$ decay due to the interference between the direct decay and the decay including $B_s^0 - \bar{B}_s^0$ mixing. The violation is described by the mixing phase ϕ_s and the difference between decay widths Γ_L and Γ_H of the light and heavy mass eigenstates $\Delta\Gamma_s = \Gamma_L - \Gamma_H$. The phase ϕ_s is related to the CKM matrix elements: $\phi_s \simeq 2\arg[(V_{ts}V_{tb}^*)/(V_{cs}V_{cb}^*)]$ and can be calculated in the SM with a very high precision:

$$\begin{aligned}\phi_s^{\text{CKMFitter}}[1] &= -0.03696^{+0.00072}_{-0.00082}\\ \phi_s^{\text{UTfit}}[2] &= -0.03700 \pm 0.00104\end{aligned}$$

One of the possible NP scenarios expects an increase of the ϕ_s value and a decline of $\Delta\Gamma_s$ [3].

*e-mail: marek.biros@cern.ch

2 Data selection

The measurement [4] uses data of proton-proton collision data at $\sqrt{s} = 13$ TeV collected by the ATLAS detector [5] during the LHC Run 2, corresponding to an integrated luminosity of 80.5 fb^{-1}. The data are analyzed and the results are statistically combined with the older measurement with 19.2 fb^{-1} of integrated luminosity of Run 1 at $\sqrt{s} = 7$ TeV and $\sqrt{s} = 8$ TeV [6]. Preselection triggers are based on the $J/\psi \to \mu\mu$ identification with selection criteria for the transverse momentum of muons $p_{\mathrm{T}} > 4$ GeV or $p_{\mathrm{T}} > 6$ GeV [1].

Each event with a $B_s^0 \to J/\psi(\mu^+\mu^-)\phi(K^+K^-)$ candidate must contain at least one reconstructed primary vertex, formed from at least four Inner Detector (ID) tracks, and at least one pair of oppositely charged muon candidates. Muon pairs are refitted to form a J/ψ candidate vertex, requiring the quality of the vertex fit to be $\chi^2/\mathrm{ndof} < 10$ (where ndof stands for the number of degrees of freedom) and pass one of tree mass window cuts of $m(\mu\mu)$ to match the tabular J/ψ mass with the window widths based on muons pseudorapidity accounting for various mass resolution in different parts of the ATLAS detector. Two oppositely charged hadron tracks from the ID satisfying $p_{\mathrm{T}} > 1$ GeV form a ϕ meson candidate. The mass window $m(KK) \in (1008.5, 1030.5)$ MeV is required. The B_s meson candidate is reconstructed from the J/ψ candidates with $m(\mu\mu)$ constrained to the average J/ψ mass [7] and the ϕ candidates, requiring $m(B_s^0) \in (5150, 5650)$ MeV and vertex-fit $\chi^2/\mathrm{ndof} < 3$. A candidate with the smallest χ^2/ndof is selected in events with multiple B_s^0 candidates.

3 Opposite-side tagging

Knowing the flavour of the B-hadron ($B_s/\bar{B}_s$) at the time of its production, significantly increases the sensitivity of the likelihood fit model to the value of ϕ_s. For the per-candidate B_s flavour probability $P(B|Q)$, four types of taggers are used: an electron tagger, low-p_{T} and tight muon taggers and a b-jet taggers. The extracted flavour probability is then propagated into the likelihood function. The taggers are based on the charge of tracks Q_X weighted by p_{T} in a ΔR cone around the opposite-side (OS) primary object (μ, e, b-jet). Q_X is defined as:

$$Q_X = \frac{\Sigma_i^{N_{tracks}} p_{\mathrm{T}i}^{\kappa} q_i}{\Sigma_i^{N_{tracks}} p_{\mathrm{T}i}^{\kappa}},$$

where parameters ΔR and κ are tuned for every tagger separately.

The self-tagged channel of $B^{\pm} \to J/\psi K^{\pm}$ is used for calibration. The tagging performance is described by the tagging efficiency ϵ_X (the number of signal events tagged by that method divided by the total number of signal events in the sample), the dilution D_X (purity of a particular flavour tagging method), tagging power T_X (combining the efficiency and the dilution) and the effective dilution (calculated from the measured tagging power and efficiency). Values for the different taggers can be found in Table 1. The total tagging efficiency is 21.23 ± 0.03% and the total tagging power is 1.75 ± 0.01%.

4 Maximum Likelihood Fit

The time-dependent angular correlations of the $B_s^0 \to J/\psi\phi$ decay are described by thirteen physics parameters: the CPV phase ϕ_s, decay width and width difference Γ_s and $\Delta\Gamma_s$, three

[1] ATLAS uses a right-handed coordinate system with its origin at the nominal interaction point (IP) in the centre of the detector and the z-axis along the beam pipe. The x-axis points from the IP to the centre of the LHC ring, and the y-axis points upward. Polar coordinates (r, ϕ) are used in the transverse plane, ϕ being the azimuthal angle around the z-axis. The pseudorapidity is defined in terms of the polar angle θ as $\eta = -\ln\tan(\theta/2)$.

Table 1. Summary of tagging performances for the different flavour tagging methods on the sample of $B^{\pm}$ signal candidates, as described in the text. Uncertainties shown are statistical only. The efficiency ϵ_X and tagging power T_X are each determined by summing over the individual bins of the cone charge distribution. The effective dilution D_X is obtained from the measured efficiency and tagging power. For the efficiency, effective dilution, and tagging power, the corresponding uncertainty is determined by combining the appropriate uncertainties in the individual bins of each charge distribution [4].

Tag method	ϵ_X [%]	D_X [%]	T_X [%]
Tight muon	4.50 ± 0.01	43.8 ± 0.2	0.862 ± 0.009
Electron	1.57 ± 0.01	41.8 ± 0.2	0.274 ± 0.004
Low-p_T muon	3.12 ± 0.01	29.9 ± 0.2	0.278 ± 0.006
Jet	12.04 ± 0.02	16.6 ± 0.1	0.334 ± 0.006
Total	21.23 ± 0.03	28.7 ± 0.1	1.75 ± 0.01

CP-state amplitudes $|A_0(0)|^2$, $|A_\perp(0)|^2$ and $|A_\parallel(0)|^2$, three strong phases δ_0, $\delta_\parallel$ and $\delta_\perp$, S-wave amplitude and phase $|A_S(0)|^2$ and δ_S, mass difference Δm_s and λ. Nine of them were extracted from the fit using the unbinned maximum likelihood method, while the size of the remaining amplitude $|A_\perp(0)|^2$ is constrained by the normalisation condition, the phase δ_0 is set to zero, the mass difference Δm_s was fixed to the world average value [7] (since that value is more precise than the ATLAS sensitivity) and λ value was fixed to 1 (assuming there is no direct CPV contribution). The observables in the fit are the reconstructed mass of the B_s^0-candidate m and its uncertainty σ_m, the proper decay time t with the uncertainty σ_t, the measured transverse momentum p_{T}, transversity decay angles $\Omega = (\theta_T, \psi_T, \phi_T)$ and the tagging probability $P(B|Q)$. Using B_s^0-candidate mass (m_i) is beneficial for the better signal-background separation, while observables σ_{m_i}, σ_{t_i}, $p_{\mathrm{T}i}$ are conditional observables allowing to precisely model the detector resolution. The likelihood is defined as follows:

$$\begin{aligned}\ln\,\mathcal{L} = \sum_{i=1}^{N_{events}} \{ & w_i \cdot \ln(f_{\mathrm{s}} \cdot \mathcal{F}_{\mathrm{s}}(m_i, t_i, \sigma_m, \sigma_t, \Omega_i, P(B|Q), p_{\mathrm{T}_i}) \\ & + f_{\mathrm{s}} \cdot f_{B_d^0} \cdot \mathcal{F}_{B_d^0}(m_i, t_i, \sigma_m, \sigma_t, \Omega_i, P(B|Q), p_{\mathrm{T}_i}) \\ & + f_{\mathrm{s}} \cdot f_{\Lambda_b} \cdot \mathcal{F}_{\Lambda_b}(m_i, t_i, \sigma_m, \sigma_t, \Omega_i, P(B|Q), p_{\mathrm{T}_i}) \\ & + (1 - f_{\mathrm{s}} \cdot (1 + f_{B_d^0} + f_{\Lambda_b})) \cdot \mathcal{F}_{\mathrm{bkg}}(m_i, t_i, \sigma_m, \sigma_t, \Omega_i, P(B|Q), p_{\mathrm{T}_i}))\}.\end{aligned}$$

The proper decay time efficiency weights w_i are introduced to compensate for the detection inefficiencies at large decay times (originating mostly in trigger-tracking limitations). $\mathcal{F}_s$ stands for the function describing the signal component, $\mathcal{F}_{bkg}$ for the combinatorial background, while peaking backgrounds $B_d \to J/\psi K^*$ and $\Lambda_b \to J/\psi p K^-$ are represented by $\mathcal{F}_{B_d^0}$ and $\mathcal{F}_{\Lambda_b}$.

5 Results

The measured physical parameters are presented in Table 2. The precision of the measurement is predominantly driven by the statistical uncertainties. The major systematic uncertainty on ϕ_s comes from the flavour tagging procedure. Two possible solutions (denoted as solution (a) and solution (b), the order is arbitrary) were obtained for the strong phases $\delta_\parallel$ and $\delta_\perp$, while the other physics parameters remain the same for the two solutions. The comparison of the measured physics parameters with the SM prediction and with other measurements

is shown in Figure 1. Fit projections for the mass, the proper decay time and the transversity angles, are shown in Figure 2. The differences between the fit and the data weighted by the combined uncertainty (statistical and systematical uncertainties summed in quadrature) in each bin is shown below each figure. The deviations are within 2σ range, which indicates a good agreement between the data and the fit model.

Table 2. Values of the physical parameters extracted in the combination of solution (a) and solution (b) of $\sqrt{s}$=13 TeV results with those obtained from $\sqrt{s}$=7 TeV and $\sqrt{s}$=8 TeV data [4].

Parameter	Solution (a)			Solution (b)		
	Value	Statistical uncertainty	Systematic uncertainty	Value	Statistical uncertainty	Systematic uncertainty
ϕ_s [rad]	−0.087	0.036	0.021	−0.087	0.036	0.021
$\Delta\Gamma_s$ [ps^{-1}]	0.0657	0.0043	0.0037	0.0657	0.0043	0.0037
Γ_s [ps^{-1}]	0.6703	0.0014	0.0018	0.6704	0.0014	0.0018
$\lvert A_\parallel(0)\rvert^2$	0.2220	0.0017	0.0021	0.2218	0.0017	0.0021
$\lvert A_0(0)\rvert^2$	0.5152	0.0012	0.0034	0.5152	0.0012	0.0034
$\lvert A_S\rvert^2$	0.0343	0.0031	0.0045	0.0348	0.0031	0.0045
$\delta_\perp$ [rad]	3.22	0.10	0.05	3.03	0.10	0.05
$\delta_\parallel$ [rad]	3.36	0.05	0.09	2.95	0.05	0.09
$\delta_\perp - \delta_S$ [rad]	−0.24	0.05	0.04	−0.24	0.05	0.04

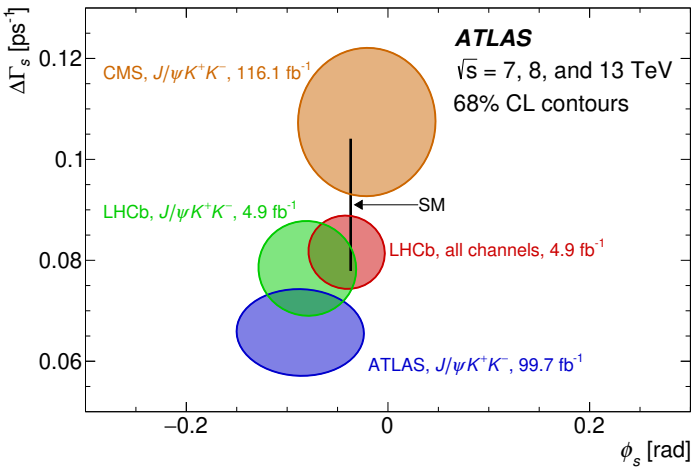

Figure 1. Contours of 68% confidence level in the $\phi_s - \Delta\Gamma_s$ plane, including results from CMS (orange) [8] and LHCb (green) [9] using the $B_s \to J/\psi\phi$ decay only and LHCb (red) [10–13] for all the channels. The SM prediction [14, 15] is shown as a thin black rectangle. Statistical and systematic uncertainties are combined in quadrature. Figure taken from Ref. [4].

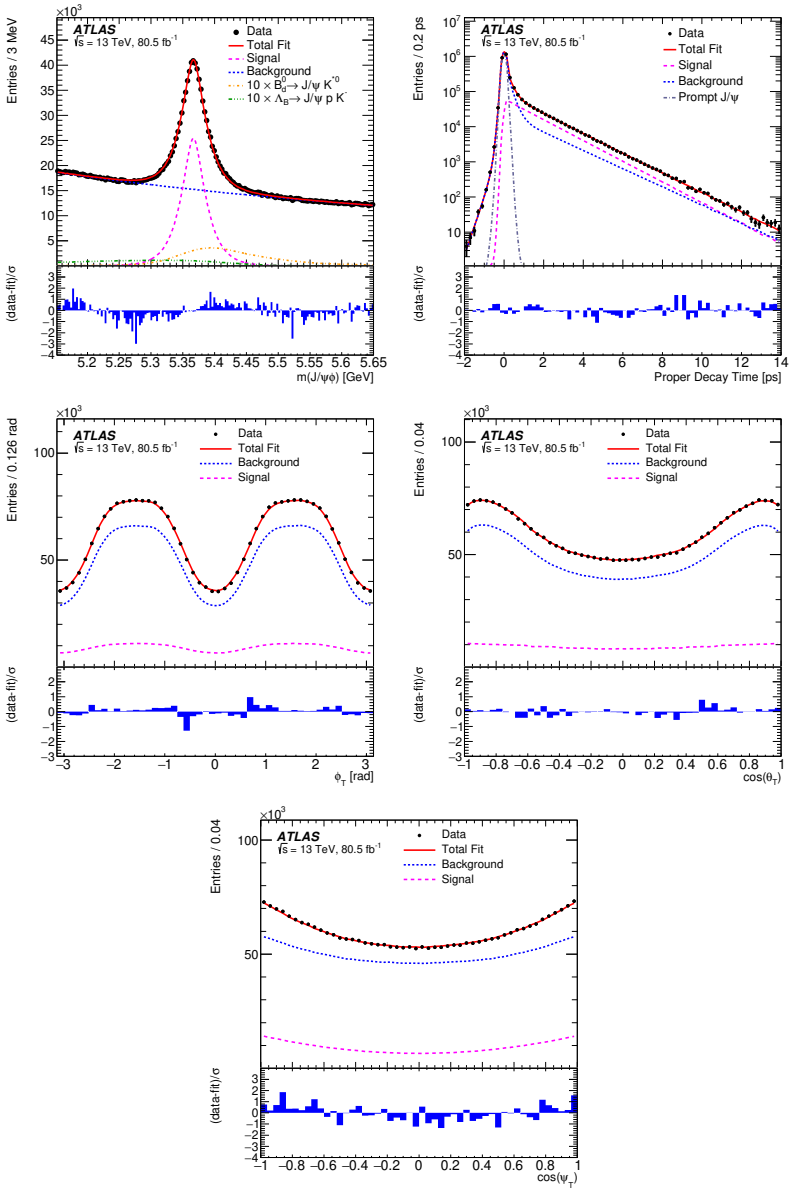

Figure 2. Mass and proper decay time (top), the transversity angles ϕ_T, $\cos(\theta_T)$, and $\cos(\psi_T)$ (bottom) projections of the final fit and its components. The red and dashed magenta lines show the total fit and the signal component. The blue dotted line shows the total background on all plots except for the mass fit projection where it represents the combinatorial background only, while $B_d^0 \to J/\psi K^{*0}$ and $\Lambda_b \to J/\psi p K^-$ backgrounds are separately represented by the orange dash-dotted and green dash-dot-dotted lines. The dashed grey line on the proper decay time projection represents the prompt J/ψ background. For the mass projection, the combinatorial background, the $B_d \to J/\psi K^*$ and $\Lambda_b \to J/\psi p K^-$ components are shown as a blue dotted line, the orange dash-dotted line and the green dash-dot-dot line, respectively. For the proper decay time and the tranversity angles, the blue dotted line and a dashed grey line show the total background and the prompt J/ψ background component. Figure taken from Ref. [4].

6 HL-LHC prospects

The key variable for a precise CPV measurement is the proper decay time t, therefore the most important parameters of the detector are the resolution and the bias of the proper decay time, in particular the performance in the expected harsh environment of high pile-up. The proper decay time resolution and bias are presented as a function of the number of reconstructed primary vertices and transversal momenta of the B candidate. Comparisons are made between the Run-1, Run-2 and HL-LHC Monte Carlo (MC) simulations (including the full simulation and reconstruction chain) and illustrated in Figures 3 and 4. The main upgrade of ATLAS between Run 1 and Run 2 was the insertable B-Layer (IBL) [16]: a new innermost layer of the ID. Before HL-LHC, ATLAS will undergo major upgrade, including also a full replacement of the ID by a new pixel and strips based silicon-detectors tracker (ITk) [17]. Figure 5 illustrates the expected precision of the $B_s^0 \to J/\psi\phi$ measurement at the HL-LHC.

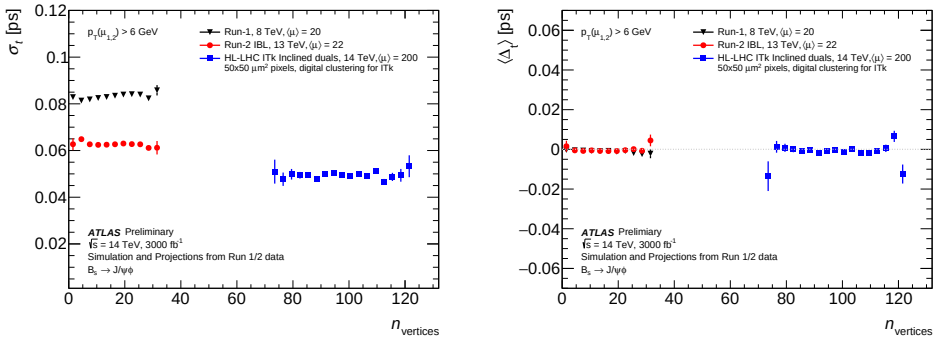

Figure 3. Dependence of the MC-true based proper decay time resolution (left) and bias of the proper decay time reconstruction (right) of the $B_s \to J/\psi\phi$ on the number of reconstructed primary vertices. Run 1 (ID), Run 2 (IBL) and upgrade HL-LHC MC simulations are included for comparison. All these samples use 6 GeV muon p_T cuts. Figure taken from Ref.[18].

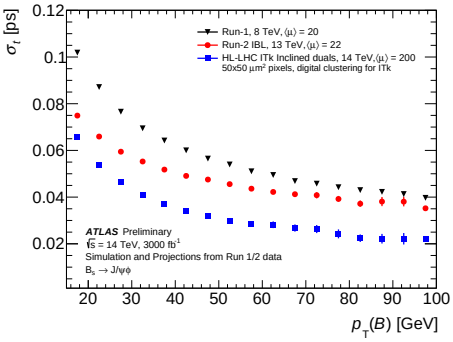

Figure 4. Dependence of the proper decay time resolution of the B_s^0 meson of the signal $B_s \to J/\psi\phi$ on p_T. Per-candidate resolutions corrected for scale factors are shown, comparing the performance in Run 1 (ID), Run 2 (IBL) and upgrade HL-LHC MC simulations. All samples use 6 GeV muon p_T cuts. Figure taken from Ref. [18].

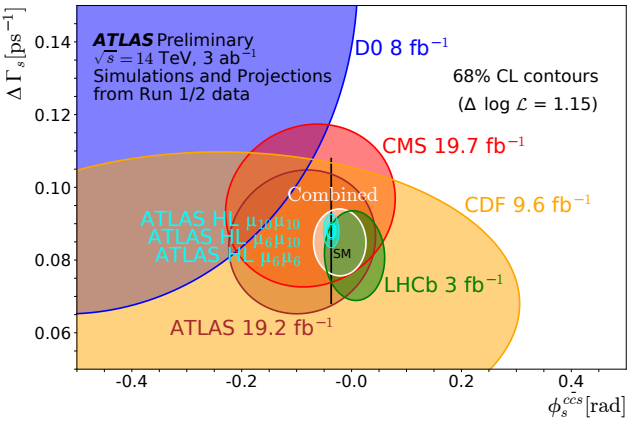

Figure 5. Current experimental summary of the ϕ_s measurements with superimposed ATLAS HL-LHC extrapolations, including both the projected statistical and systematic uncertainties. The three ATLAS extrapolations account for optimistic, intermediate and conservative trigger scenarios (varying the muon p_{T} trigger thresholds). Figure taken from Ref. [18].

7 Summary

Results of the ATLAS measurement with a dataset corresponding to an integrated luminosity of 80.5 fb^{-1} at $\sqrt{s} = 13$ TeV are statistically combined with the previous results with a dataset corresponding to an integrated luminosity of 19.2 fb^{-1} at $\sqrt{s} = 7$ TeV and $\sqrt{s} = 8$ TeV. The value of the most sensitive parameter to the New Physics phenomena ϕ_s is presented: $\phi_s = -0.087 \pm 0.036(\mathrm{stat.}) \pm 0.021(\mathrm{syst.})$. Results are generally consistent with the Standard Model prediction and LHCb and CMS measurements, with the exception of $\Delta\Gamma_s$ that shows 3σ tension concerning the current world combined value. The expected ATLAS detector performance after the HL-LHC upgrade was simulated and the projection of the precision of the measurement is presented. The improvement in ϕ_s statistical uncertainty (w.r.t. Run 1) ranges between a factor 9 and 20 depending on the trigger scenario.

Acknowledgement

This work was supported by the Ministry of Education, Youth and Sports of the Czech Republic under grant LM2023040, and by Charles University grants UNCE/SCI/013 and SVV No. 260713.

References

[1] J. Charles et al. (CKMfitter Group), *Current status of the standard model CKM fit and constraints on $\Delta F = 2$ new physics*, Phys. Rev. D 91 (2015) 073007

[2] M. Bona et al. (UTfit Collaboration), *The unitarity triangle fit in the standard model and hadronic parameters from lattice QCD: a reappraisal after the measurements of Δm_s and BR($B \to \tau\nu_\tau$)*, JHEP 10 (2006) 081

[3] A. Lenz and U. Nierste, *Theoretical update of $B_s - \bar{B}_s$ mixing*, JHEP 06 (2007) 072

[4] ATLAS Collaboration, *Measurement of the CP-violating phase ϕ_s in $B_s^0 \to J/\psi\phi$ decays in ATLAS at 13 TeV*, Eur. Phys. J. C 81 (2021) 342

[5] ATLAS Collaboration, *The ATLAS Experiment at the CERN Large Hadron Collider*, JINST 3 (2008) S08003.

[6] ATLAS Collaboration, *Measurement of the CP-violating phase ϕ_s and the B_s^0 meson decay width $B_s^0 \to J/\psi\phi$ difference with decays in ATLAS*, JHEP 08 (2016) 147

[7] P. A. Zyla et al. (Particle Data Group), *Review of Particle Physics*, Prog. Theor. Exp. Phys. (2020) 083C01

[8] CMS Collaboration, *Measurement of the CP-violating phase ϕ_s in the $B_s^0 \to J/\psi\phi(1020) \to \mu^+\mu^- K^+K^-$ channel in proton– proton collisions at $\sqrt{s} = 13$ TeV*, Phys. Lett. B 816 (2021) 136188

[9] LHCb Collaboration, *Updated measurement of time-dependent CP-violating observables in $B_s^0 \to \psi(2S)K^+K^-$ decays*, Eur. Phys. J. C 79 (2019) 706 [Erratum: Eur. Phys. J. C 80 (2020) 601]

[10] LHCb Collaboration, *First study of the CP-violating phase and decay-width difference in $B_s^0 \to \psi(2S)\phi(1020)$ decays*, Phys. Lett. B 762 (2016) 253

[11] LHCb Collaboration, *Measurement of the CP-violating phase ϕ_s in the $\bar{B}_s^0 \to D_s^+ D_s^-$ decays*, Phys. Rev. Lett. 113 (2014) 211801

[12] LHCb Collaboration, *Measurement of the CP-violating phase ϕ_s in the $\bar{B}_s^0 \to J/\psi\pi^+\pi^-$ decays*, Phys. Lett. B 736 (2014) 186

[13] LHCb Collaboration, *Measurement of the CP-violating phase ϕ_s from $B_s^0 \to J/\psi\pi^+\pi^-$ decays in 13 TeV pp collisions*, Phys. Lett. B 797 (2019) 134789

[14] A. Lenz and G. Tetlalmatzi-Xolocotzi, *Model-independent bounds on new physics effects in non-leptonic tree-level decays of B-mesons*, J. High Energ. Phys. (2020) 177

[15] J. Charles et al. (CKMfitter Group), *Current status of the Standard Model CKM fit and constraints on $\Delta F = 2$ New Physics*, Phys. Rev. D 91 (2015) 073007

[16] ATLAS Collaboration, *ATLAS insertable B-layer technical design report*, CERN-LHCC-2010-013, ATLAS-TDR-19, (2010)

[17] ATLAS Collaboration, *Technical Design Report for the ATLAS Inner Tracker Pixel Detector*, CERN-LHCC-2017-021, ATLAS-TDR-030 (2017)

[18] ATLAS Collaboration, *CP-violation measurement prospects in the $B_s^0 \to J/\psi\phi$ channel with the upgraded ATLAS detector at the HL-LHC*, ATL-PHYS-PUB-2018-041 (2018)